

FLEXIBLE DIGITAL MODULATION AND CODING SYNTHESIS FOR SATELLITE COMMUNICATIONS

Mark Vanderaar*
Sverdrup Technology, Inc.
2001 Aerospace Parkway
Brookpark, Ohio 44142

James Budinger
NASA Lewis Research Center
Mail Stop 54-8
21000 Brookpark Rd.
Cleveland, Ohio 44135

Craig Hoerig and Dr. John Tague**
Dept. of Electrical and Computer
Engineering
Ohio University
Athens, Ohio 45701

ABSTRACT

This paper presents an architecture and a hardware prototype of a Flexible Trellis Modem / Codec (FTMC) transmitter. The theory of operation is built upon a pragmatic approach to trellis-coded modulation that emphasizes power and spectral efficiency [1]. The system incorporates programmable modulation formats, variations of trellis-coding, digital baseband pulse-shaping, and digital channel precompensation. The modulation formats examined include (uncoded and coded) Binary Phase Shift Keying (BPSK), Quaternary Phase Shift Keying (QPSK), Octal Phase Shift Keying (8PSK), 16-ary Quadrature Amplitude Modulation (16-QAM), and Quadrature Quadrature Phase Shift Keying (Q^2 PSK) at programmable rates up to 20 Megabits per second (Mbps). The FTMC is part of a developing test bed to quantify modulation and coding concepts.

INTRODUCTION

Regenerative transponders employing onboard-processing and switching techniques are active topics in satellite communications [2, 3, 4]. One common feature among the architectures proposed is the presence of modems and codecs both on the ground and in the spacecraft. The modems and codecs are used with multiple access schemes designed to optimize both uplink and downlink capacities. Generally, they trade some mix of bandwidth and power efficiency.

Frequency Division Multiple Access (FDMA) is an appropriate multiple access technique for low-rate bandwidth efficient uplinks from a large number of ground terminals. In this type of uplink, bandwidth efficiency is directly related to the amount of uplink traffic attainable. Time Division Multiplexing (TDM) is envisioned in high-rate downlinks for its power efficiency. In TDM, nonlinear High Power Amplifiers (HPA's) can be operated at saturation without the adverse effect of intermodulation and distortion as long as the modulated signal maintains a constant envelope. Spread spectrum techniques such as Code Division Multiple Access (CDMA) are used for their power efficiency for the same reasons as TDM. CDMA has also shown increased spectral efficiency in some systems and may be suitable for both uplinks and downlinks.

In the future, as data throughput requirements increase to offer wider band services, TDM or CDM downlinks may not only be limited by available transmit power but also by channel, transponder, and ground terminal bandwidths. For

*Work Supported by Contract NAS3-25266, Task Order 5601, Digital Systems Technology Development.

**Work Supported by Grant NAG3-1183, High Precision Waveform Equalization for Optimum Digital Signalling.

example, Travelling Wave Tube Amplifiers (TWTAs) qualified for space environments today exhibit bandwidths on the order of 1 to 5 percent of the operating frequency [5]. Higher output power TWTAs generally afford lower bandwidth percentages. Technologies such as electronically steerable phased arrays that employ patch antennas can be designed to exhibit bandwidths on the order of 10 percent of their operating frequencies, though they become simpler and smaller at more modest bandwidths of 1 to 3 percent. Also, digital modem and codec hardware can be designed to operate almost exclusively at the symbol rate, as opposed to the bit rate. Thus, higher bit throughput rates can be accomplished at lower processing rate by using modulation schemes with more bits per symbol. This may be useful in a TDM downlink exhibiting high rates to a number of low-cost ground terminals.

Increased flexibility is another dimension in future satellite systems. The on-orbit reconfiguration of the modulation and coding hardware offers the potential to provide more network capacity, increased network availability, multiple service classes, and higher percentage availability at the expense of increased complexity. Efficient use of capacity could be obtained with a network that charges users for the amount of network resources required. Users that require high data and low error rate services would expend more channel bandwidth and/or power per transmitted bit than user with lower quality and rate service requirements. Wider availability may be obtained with flexible transmission formats suited to particular user requirements. Higher percentage availability may be achieved by reconfiguring to more conservative modulation and coding formats overcoming outages such as rain attenuation and multipath fading at the expense of network capacity.

This set of possible operating environments warrant the investigation of modems and codecs that can offer future satellite systems increased operational performance and flexibility.

The first section of this paper presents an overview of the modulation and coding test bed under development. The second section describes the modulation and coding formats supported by the FTMC. The next section develops the digital pulse shaping techniques. Digital baseband precompensation methods for nonlinear channel distortion are then described. The prototype transmitter that includes the baseband modulator and IF upconversion is described next. Finally, conclusions are drawn as to the applicability of the techniques presented.

SYSTEM CONFIGURATION

Though this paper focuses on the FTMC transmitter, a brief description is given of the test bed under development. The

proposed FTMC test bed architecture is shown in Figure 1. System control is performed through a personal computer that features a graphical user interface for ease of system configuration and operation. FTMC configuration data is generated via object-oriented simulation software on a workstation. The real time data flow through the FTMC begins with either Pseudo-Random Binary Sequence (PRBS) or patterned test data generated by a digital transmission analyzer (DTA). The DTA is clocked with the FTMC modulator hardware at the programmed data rate. TDM formatting is done by the burst controller. The baseband modulated waveform is then generated by the FTMC modulator. Translation to a 70 MHz IF is performed through quadrature upconversion techniques. The data can then either be translated to RF for amplification via a TWTA or directly to a calibrated IF noise combiner. The signal is then downconverted to baseband where it is filtered, demodulated, and decoded by the FTMC demodulator currently under development.

$$m_I(t) = h(t) * s_I(t)$$

$$m_Q(t) = h(t) * s_Q(t)$$

where $s_I(t)$ and $s_Q(t)$ are the information carrying signals. The information carrying signals can be represented as square pulses over the symbol time T_s of an amplitude corresponding to the constellation definition. The function $h(t)$ is the impulse response of the bandlimiting pulse shape and is described in the next section. Convolution is denoted by the $*$ symbol. In the case of Q^2PSK the information carrying signals correspond to the following expressions

$$s_I(t) = a_1(t)*p_1(t) + a_2(t)*p_2(t)$$

$$s_Q(t) = a_3(t)*p_1(t) + a_4(t)*p_2(t)$$

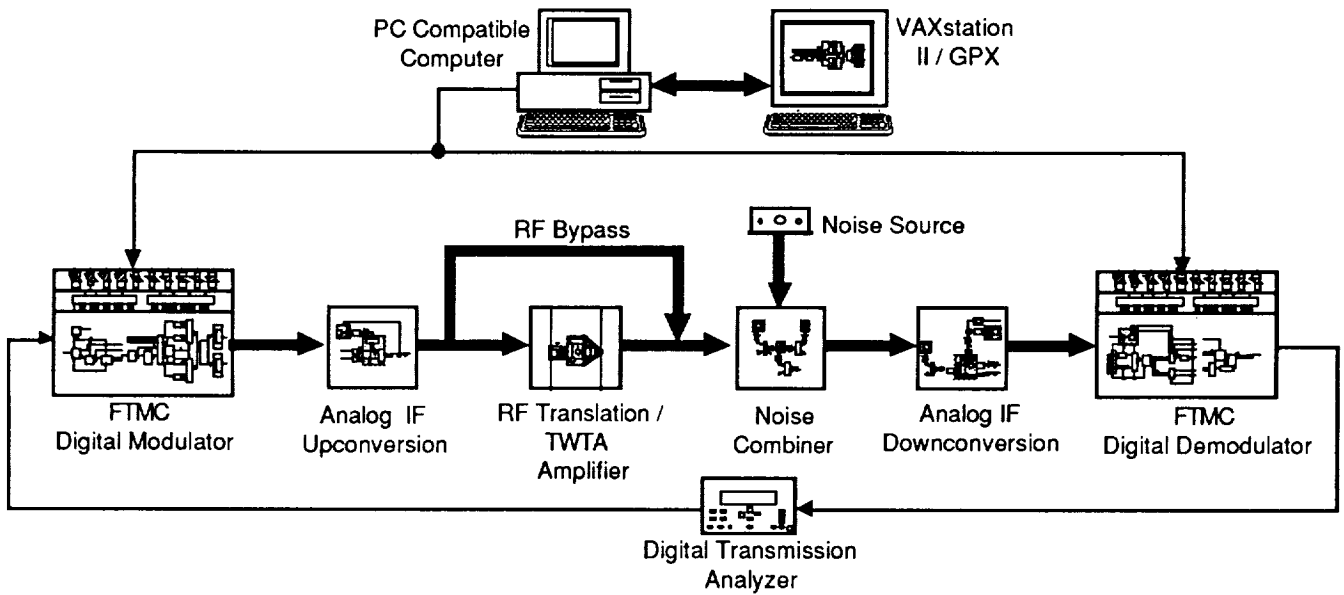


Figure 1. FTMC Test Bed

MODULATION AND CODING

The FTMC supports a number of different modulation formats. Each can be represented in quadrature form by the equation

$$x_{tx}(t) = m_I(t)\cos(2\pi f_c t) + m_Q(t)\sin(2\pi f_c t)$$

where $x_{tx}(t)$ denotes the resulting modulation at a carrier frequency f_c . The signals $m_I(t)$ and $m_Q(t)$ represent the baseband modulating functions. Three Phase Shift Keyed (PSK) techniques are supported that include BPSK, QPSK, and 8PSK. An amplitude and phase modulated technique, 16-QAM, as well as a phase and pulse-shape modulated technique Q^2PSK [6], are also supported. In the PSK and QAM cases the baseband modulating functions represent the in-phase and quadrature bandlimited values associated with the signalling constellation. These can be written as

where each $a_n(t)$ corresponds to a positive or negative amplitude, depending on the information sequence. The $p_1(t)$ and $p_2(t)$ are a set of two orthogonal pulse shapes that also maintain orthogonality with the quadrature mixing operation. These conditions can be defined explicitly by the relations

$$\int_{nT_s}^{(n+1)T_s} p_1(t)p_2(t)dt = 0$$

$$\int_{nT_s}^{(n+1)T_s} p_i(t)e^{j2\pi f_c t}dt = 0, \quad i=1,2$$

$$f_c = \left(\frac{m}{2T_s} \right), \quad m = \text{integer} \geq 1$$

where n is an integer to define integration over any symbol time. There are an infinite number of $p_i(t)$'s that satisfy the above conditions. A few are developed in [6] that address the issue of phase continuity as well as spectral occupancy. In general, any modulation format whose $S_I(t)$ and $S_Q(t)$ can be represented by two or fewer bits can be created by the FTMC modulator. This is clarified in the waveform synthesis section.

The bit to symbol mapping of all the modulation formats are designed to operate in conjunction with a standard convolutional code of constraint length $K=7$ and rate $1/2$ with generator polynomials $G_{11}=133_g$ and $G_{12}=171_g$ exhibiting the maximal attainable d_{free} of 10 (Figure 2). This approach allows the use of a single encoder and decoder to be used with the programmable modulation formats to achieve a 3 to 7 dB coding gains at real spectral efficiencies (using 40% Nyquist pulse-shaping filters) up to 2.14 bits/second/Hz. Coding gain can be approximated accurately at lower bit-error-rates by the Asymptotic Coding Gain (ACG). The calculation of ACG is based on the most likely decoding error event. The most likely decoding error event for unmerged paths with length greater than one is called the Unmerged Squared Euclidean Distance (USED). As shown in [1] USED for MPSK can be expressed as

$$USED \geq 2 \sin^2 \left(\frac{2\pi}{M} \right) + (d_{free} - 4) \sin^2 \left(\frac{\pi}{M} \right), \quad M \geq 4$$

where M is the modulation order of the coded scheme. Codes with parallel branches (and thus single branch errors events) have a Parallel Squared Euclidean Distance (PSED), again for MSPK, expressed as

$$PSED \geq \sin^2 \left(\frac{4\pi}{M} \right), \quad M \geq 8$$

ACG is defined as the ratio of the minimum of the USED or PSED to the Normalized Euclidean Distance (NED) for uncoded performance. NED can be written as

$$NED = \sin^2 \left(\frac{2\pi}{M} \right)$$

and thus the ACG (in dB) for MPSK is

$$ACG \geq 10 \log_{10} \left\{ 4 \min \left[\cos^2 \left(\frac{2\pi}{M} \right), \frac{1}{2} + \frac{3}{8 \cos^2 \left(\frac{\pi}{M} \right)} \right] \right\}$$

Evaluations of this expression are given in Table 1. Uncoded performance was calculated using standard bounds [7, 8] for gray coded mappings. Note that for $M=4$ ACG is determined by the USED and for $M=8$ ACG is determined by the PSED. A similar argument will be discussed to evaluate QAM performance.

Modulation Format	Code Rate(s)	Asymptotic Coding Gain	$\sim E_b/N_0$ for $P_b = 10^{-6}$	Spectral Efficiency*
BPSK	NA	NA	10.5 dB	0.72
QPSK	NA	NA	10.5 dB	1.43
8PSK	NA	NA	14.0 dB	2.14
16QAM	NA	NA	14.4 dB	2.86
TQPSK	1/2	7.0 dB	4.5 dB	0.72
T8PSK	2/3	3.0 dB	7.5 dB	1.43
T16QAM	2/4	4.3 dB	6.5 dB	1.43
T16QAM	3/4	3.6 dB	10.4 dB	2.14

* In bits/sec/Hz assuming 40% Nyquist Filtering

Table 1 : Modulation and Coding Performance

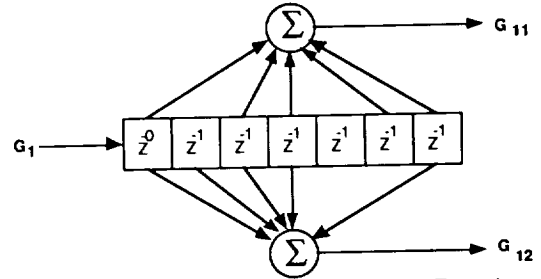


Figure 2 : Rate 1/2, k=7 Convolutional Encoder

The particulars of each coding scheme can be described by a generator matrix of the form

$$G_{n \times k} = \begin{bmatrix} G_{11} & G_{12} & \dots & G_{1k} \\ G_{21} & \dots & \dots & G_{2k} \\ \vdots & \vdots & \vdots & \vdots \\ G_{n1} & G_{n2} & \dots & G_{nk} \end{bmatrix}$$

where n is the number of input bits and k is the number of output bits from the encoder. The G_{ij} 's are the activated convolutional encoder shift register taps written in an octal form. The k output bits are mapped into a 2^k -ary modulation scheme in a manner that maximizes the Euclidean distance of the code. For trellis-coded QPSK (TQPSK) the generator matrix is

$$G_{1 \rightarrow 2} = [133_8 \quad 171_8]$$

Each information bit is coded into one QPSK symbol. A gray mapping of the encoded bits is used. For this code the ACG is determined by the USED of the seven symbol long error event path. The code and mapping structure is illustrated in Figure 3. Note the encoder output bits read from the top to bottom correspond to the bit to symbol assignments read from left to right.

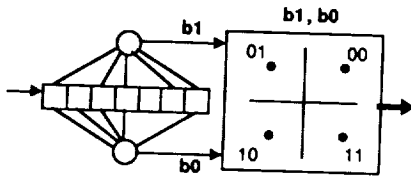


Figure 3. Trellis Coded QPSK

Similarly, for T8PSK and T16QAM the generator matrices are

$$G_{2 \rightarrow 3} = \begin{bmatrix} 133_8 & 171_8 & 0 \\ 0 & 0 & 100_8 \end{bmatrix}$$

$$G_{3 \rightarrow 4} = \begin{bmatrix} 133_8 & 171_8 & 0 & 0 \\ 0 & 0 & 100_8 & 0 \\ 0 & 0 & 0 & 100_8 \end{bmatrix}$$

The code and mapping structures are shown in Figures 4 and 5.

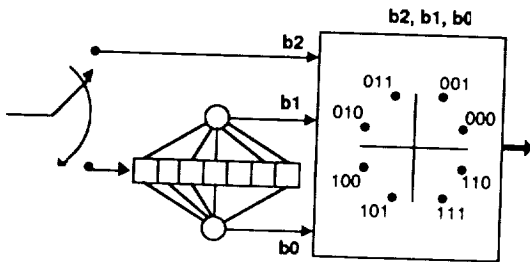


Figure 4: Trellis Coded 8PSK

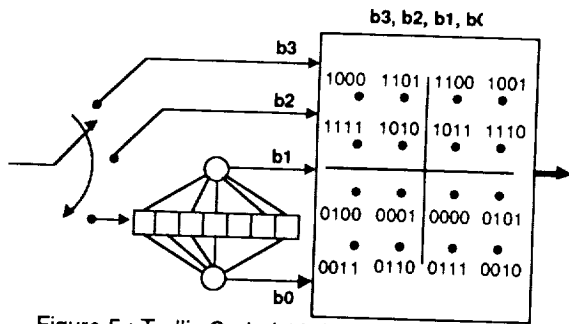


Figure 5: Trellis Coded 16-QAM (Mapping #1)

Additionally, a rate 2/4 time-varying code is supported for the 16QAM modulation format. This code maps two information bits into one of 16 modulation points. The first bit is encoded into a two bit symbol that determines the quadrant of the 16-ary symbol. The second information bit is encoded into a two bit symbol that chooses a "sector" within the previously chosen quadrant. This sector and quadrant determine a constellation point for the 16QAM format. The generator matrix is written as

$$G_{2 \rightarrow 4} = [133_8 \ 171_8] \subset [133_8 \ 171_8]$$

where \subset denotes a demultiplexing operation. The constellation mapping and the code structure is illustrated in Figure 6.

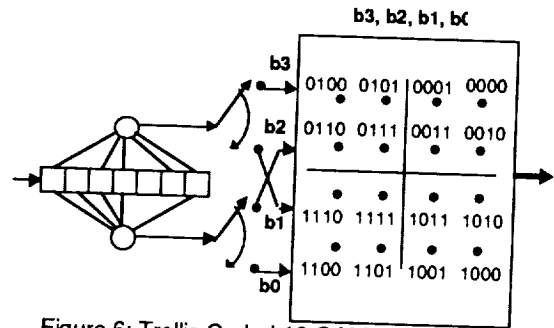


Figure 6: Trellis Coded 16 QAM (Mapping #2)

For Mapping #1 the PSED is the dominated error event. However, it is difficult to calculate due to the nature of the decision regions. However, its performance is given in [1] as approximately 10.4 dB E_b/N_0 required to obtain a bit-error-rate of 10^{-6} . This is a coding gain of 3.6 dB as compared to gray coded 8PSK.

For Mapping #2 there are no parallel paths so the PSED is not an issue. The approximate USED is 1.34 as calculated by comparing the first error event path with the all zero path in the trellis diagram. The ACG as compared to the NED of QPSK is

$$ACG \geq 10 \log_{10} \left[\frac{USED}{NED} \right] \approx 10 \log_{10} \left[\frac{1.34}{\sin^2 \left(\frac{\pi}{4} \right)} \right] = 4.3 \text{ dB}$$

WAVEFORM SYNTHESIS

To reduce spectral occupancy, a Static Random Access Memory (SRAM) Distributed Arithmetic (DA) technique is used to synthesize precision baseband pulse-shapes [9, 10, 11]. 40 and 20 percent square-root and full Nyquist raised cosine waveforms have thus far been generated at baseband by sampling and storing the appropriate combinations of transmitted data patterns. The full Nyquist pulse patterns were generated for testing purposes only. The data were sequentially generated for all symbol combinations over specified symbol apertures. An aperture is the length of time for a specified number of symbols to occur.

The frequency response of the square root raised cosine function (SRRCF) is defined by

$$H(f) = \begin{cases} \frac{\pi T_s}{\pi(1-\beta) + 4\beta}, & 0 \leq \left| \frac{f}{f_H} \right| \leq 1-\beta \\ \frac{\pi T_s}{\pi(1-\beta) + 4\beta} \cos \left[\frac{\pi}{4\beta} \left(\left| \frac{f}{f_H} \right| - 1 + \beta \right) \right], & 1-\beta \leq \left| \frac{f}{f_H} \right| \leq 1+\beta \\ 0, & 1+\beta \leq \left| \frac{f}{f_H} \right| \end{cases}$$

where T_s is the symbol period in seconds, β is the rolloff rate, and f_H is the half-amplitude frequency which equals $1/2T_s$. Taking the inverse Fourier transform of equation $H(f)$, the impulse response is found to be

$$h(t) = \left[\frac{4\beta}{\pi(1-\beta) + 4\beta} \right] \left[\frac{T_s \sin \left[\frac{\pi(1-\beta)t}{T_s} \right]}{4\beta t} + \frac{\cos \left[\frac{\pi(1+\beta)t}{T_s} \right] + \frac{4\beta t}{T_s^3} \sin \left[\frac{\pi(1-\beta)t}{T_s} \right]}{1 - \left(\frac{4\beta t}{T_s} \right)^2} \right]$$

where $h(0) = 1$ and

$$h\left(\pm \frac{T_s}{4\beta}\right) = \left[\frac{4\beta}{\pi(1-\beta) + 4\beta} \right] \left[\frac{\sin \left[\frac{\pi(1-\beta)t}{4\beta} \right]}{2} + \frac{\pi \left\{ \cos \left[\frac{\pi}{4\beta} \right] + \sin \left[\frac{\pi}{4\beta} \right] \right\}}{4\sqrt{2}} \right]$$

The rolloff rate β is expressed as a percentage and controls the trade-off between the bandwidth and pulse duration. A lower rolloff rate will allow for a narrower passband, but its impulse response will cause more ISI.

Aperture lengths of 6 and 12 symbols were investigated depending on the modulation scheme involved. Data were collected for 8, 16, and 32 samples per symbol. Each symbol was shaped with the SRRCF and the effects of adjacent pulse responses were accounted for over the center symbol period. As the aperture length is an even number, the actual data collected represent the transition from one symbol to the next. The amount of memory required to represent the full set of data on each orthogonal channel for a given modulation format is

$$\text{memory} = \text{sps} \times \text{levels}^{\text{aperture}}$$

where sps is the number of samples per symbol and levels is the number of amplitude levels on one axis of the constellation. The amount of memory can be reduced by exploiting the symmetry in certain modulation formats. The flexible aspect of this pulse shaping procedure is that data can be generated for any rolloff rate, samples per symbol, or symbol aperture length with high precision. A typical software generated eye-diagram is illustrated in Figure 7.

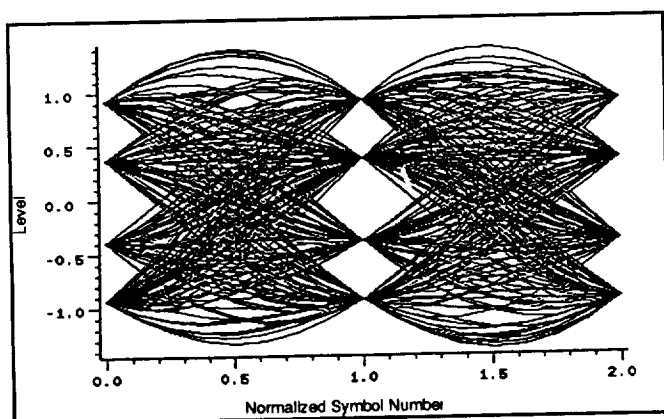


Figure 7: 8PSK Example Eye Diagram.

BASEBAND PRECOMPENSATION

Everything accomplished thus far assumes all subsequent signal transformations are ideal linear operations. However, the nonlinear responses of devices such as TWTA's distort and degrade the signalling scheme. As a second order approximation, a narrow band, frequency independent, memoryless model of a TWTA has Amplitude to Amplitude (AM/AM) and Amplitude to Phase (AM/PM) characteristics that can be modeled as

$$A(r(t)) = \frac{2r(t)}{1+r^2(t)}$$

$$\Phi(r(t)) = \Phi_0 \frac{r^2(t)}{1+r^2(t)}$$

where $r(t)$ is the input amplitude level to the TWTA. Many techniques such as precompensation, equalization, and ISI cancelling have been proposed to minimize this type of nonlinearity [12, 13, 14]. In general, transmitter precompensation can occur at baseband, IF or RF. IF and RF precompensation have been applied in many terrestrial microwave radio systems. The limitations observed in these applications are lack of flexibility, long term stability, and difficulty of accurate construction. For these reasons, there has been interest in applying digital signal processing techniques to perform baseband precompensation. Amplitude and phase distortion for an operational TWTA can be determined empirically and thus precisely precompensated. Most implementations thus far have focussed on memoryless systems that warp the signalling constellation with an inverse transform of the amplitude and phase response of the TWTA nonlinearity. However, in systems using pulse shaping, the r becomes $r(t)$ causing the warping to introduce additional ISI that results in degraded bit-error-rate performance and spectral regrowth. This problem can be solved by using a memory based architecture [15] similar to the pulse shaping technique. This technique reduces ISI accurately to the symbol aperture. It is interesting to note that this technique is well suited for satellite communications that use lower order modulation schemes. In terrestrial microwave systems, high order modulation schemes are typical. This puts a significant limitation on the aperture and thus accuracy that can be obtained. The memory size as shown in the waveform synthesis section depends exponentially on the number of discrete amplitude levels of the constellation.

The precompensation is implemented in terms of signal space vectors relative to each modulation scheme. The vectors are the complex representation of the in-phase and quadrature sample values. The magnitude and phase of these vectors is precompensated for a set of data that represents the AM/AM and AM/PM characteristics of the nonlinearity. The magnitude precompensation can be accomplished by extending the linear portion of the AM/AM curve. The input signal value enters the precompensator, and the output power is found relative to the linear extension of the data. This value is then found on the actual data curve, and the corrected input backoff corresponding to this new point is output to the rest of the system. Next, the corrected input backoff is further corrected for the AM/PM characteristics of the curve. The phase shift corresponding to this input backoff is found, and this value is subtracted from the phase of the signal entering the TWTA. An example eye diagram of precompensated data for BPSK is shown in Figure 8. A square root 40 percent raised cosine pulse was used to shape the data at 16 samples per symbol with a twelve symbol aperture. Measured AM/AM and AM/PM curves from a TWTA were used to model the nonlinearity. Figure 10 shows the precompensated scatter plot. As shown in Figure 9 the precompensated data exhibits increased spectral occupancy that must be included in the bandwidth calculations for the modulation upconversion and amplification functions. The clustering and ISI effects seen in the eye diagram are products of the square root filter. A full raised cosine or matched square root raised cosines do not exhibit these effects. Figure 11 shows the eye diagram after the TWTA distortion and a matched receive finite impulse response filter with 96 taps.

This type of precompensation would be particularly useful in an operational system. A network using precompensation could adapt and load new precompensation data as nonlinear channel characteristics changed. Comparisons are being generated that compare the total degradation for a set of modulation formats as a function of input backoff, filtering, and symbol aperture for baseband precompensated signals.

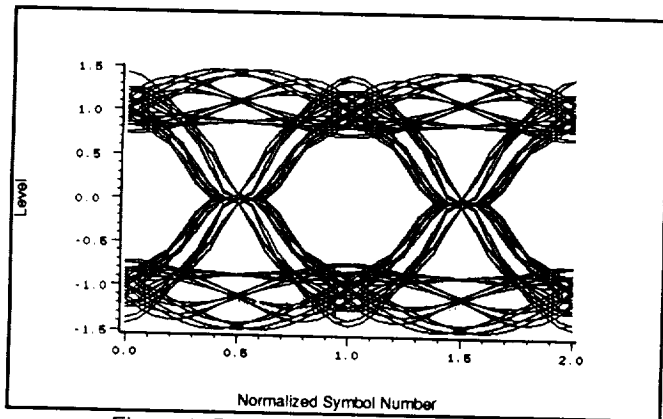


Figure 8: Precompensated eye diagram.

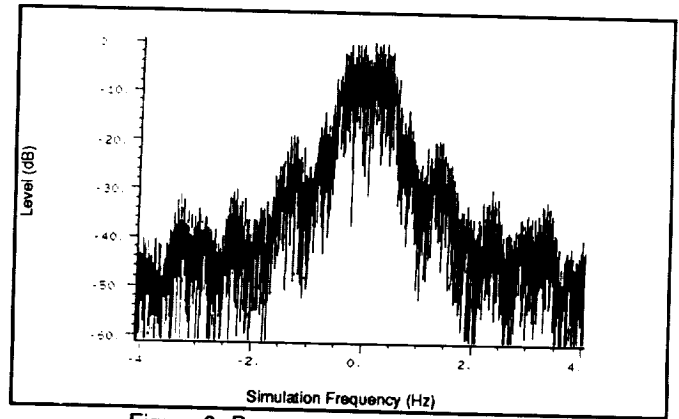


Figure 9: Precompensated spectrum.

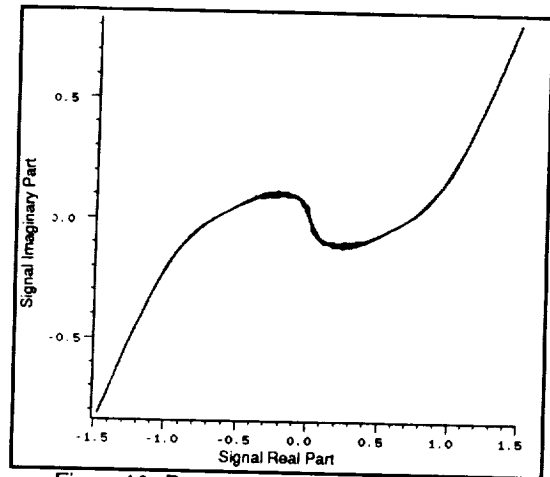


Figure 10: Precompensated scatter plot.

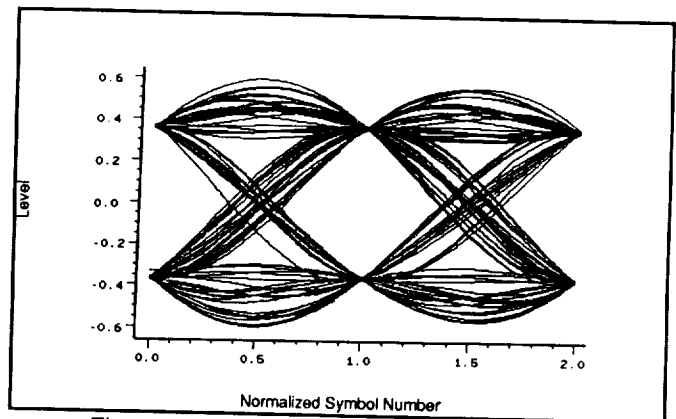


Figure 11: Receive filter output eye diagram.

FTMC TRANSMITTER HARDWARE

Prototype hardware has been constructed to verify FTMC concepts with real system nonidealities. The transmitter block diagram is shown in Figure 12 and the FTMC modem chassis layout in Figure 13. Serial data can be clocked in at TTL levels continuously or in a burst format. This data is then translated to a parallel format of one to four bits wide. One bit is supplied to the rate 1/2 k=7 convolutional encoder, and the rest bypass it. Uncoded, coded, and burst control bits (total of nine address bits) are supplied to a modulation

mapping function. This modulation mapper is a 512 X 4 bit SRAM loaded with four bits of information that represent four in-phase and four quadrature levels. This information (either data or preamble) is turned broadside to generate symbol apertures via shift registers. Symbol apertures are transformed into pulse-shaped symbols with the Nyquist pattern generators. The pattern generators are each 128K X 8 SRAM's. The SRAM's are loaded with the patterns generated via the techniques discussed in the waveform synthesis section. The eight bit samples output from the filter SRAMs are either directly output to the digital to analog converters or used as address bit to the precompensator. The precompensator performs the nonlinear transformation as described in the precompensation section. The digital to analog converters use eight bit quantization. Figures 14 through 19 show eye diagrams and spectrums of four of the modulation formats, using full 40 percent raised cosine pulse shapes. In each figure, the sample rate is 32.768 MHz and there are 32 samples per symbol. This gives a bit rate of

$$\text{Bit rate} = \frac{\text{sample rate}}{\text{samples per symbol}} \log_2(M)$$

Each spectrum is plotted in a frequency window corresponding to the width of the main lobe, $2/T_b$, of a BPSK signal with the same bit rate, where T_b is the bit time.

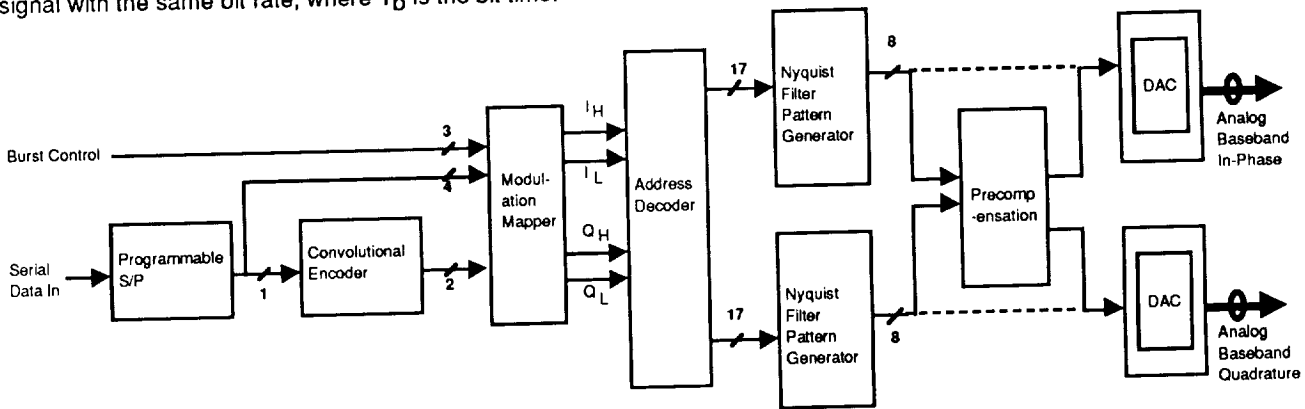


Figure 12 : Digital Baseband Modulator / Encoder

The IF upconversion module translates the baseband modulated signal to 70 MHz using standard quadrature upconversion techniques (Figure 20). The 70 MHz carrier is obtained from an analog signal generator that can be phase locked to the symbol time to satisfy Q^2 PSK orthogonality conditions. Direct Digital Synthesizers (DDS) could also be used to generate the IF carrier.

The quadrature spectral reconstruction filters are designed to accommodate the full range of FTMC operation in terms of data and sampling rate. The signal bandwidth (assuming no spectral shaping) is obtained as

$$BW = \frac{f_s}{\text{sps}}$$

where f_s is the sampling frequency and sps is the number of samples per symbol. The maximum bandwidth, BW_{max} is 5

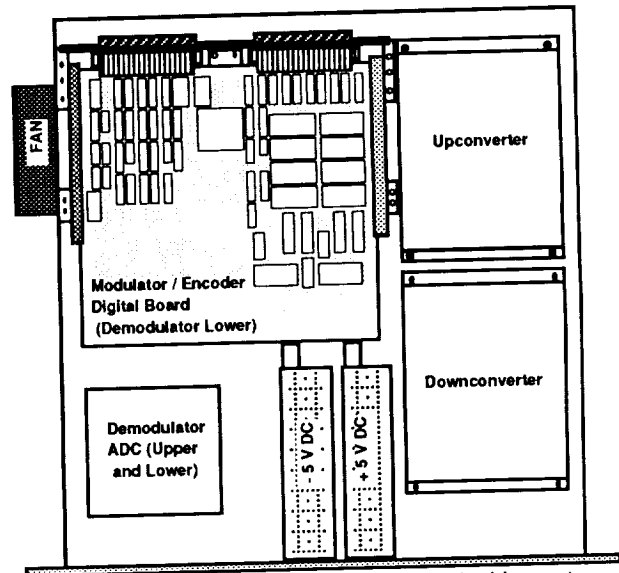


Figure 13. FMC Chassis Mechanical Layout

MHz. This occurs when f_s is 40 MHz and sps is 8 samples per symbol. The spectral reconstruction filters must contain this frequency in their passband. The other constraint defining the frequency response of the reconstruction filters is the lowest alias frequency. This occurs at $f_s = 10$ MHz and $\text{sps} = 8$, giving

$$f_{\text{alias}} = f_s - \frac{f_s}{\text{sps}} = 10 \text{ MHz} - \frac{10 \text{ MHz}}{8 \text{ sam/sym}} = 8.75 \text{ MHz}$$

This alias of 8.75 MHz must be in the stopband of the filter response. The resulting filter mask is shown in Figure 21, with the 48 dB of attenuation specification obtained from the quantization error of the 8 bit digital to analog converters. Note that the eventual limit of available sample rates and data rates is limited by the lack of flexibility in the reconstruction filter. To maintain the low level of ISI obtained by the Nyquist filters the group delay variation is limited to

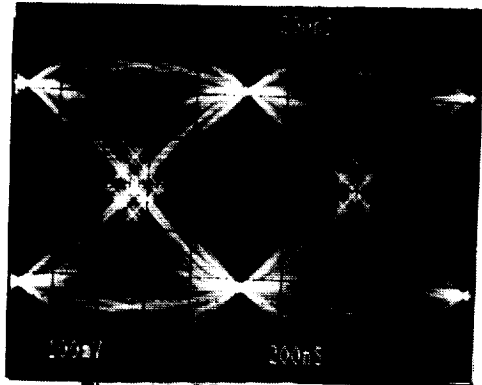


Figure14: BPSK Eye Diagram

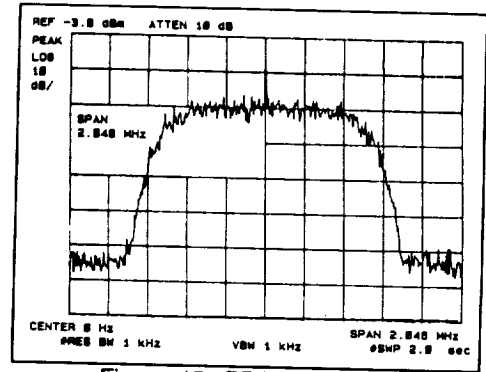


Figure 15: BPSK Spectrum

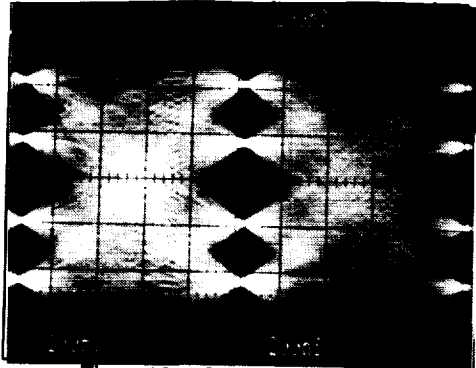


Figure16: 8PSK Eye Diagram

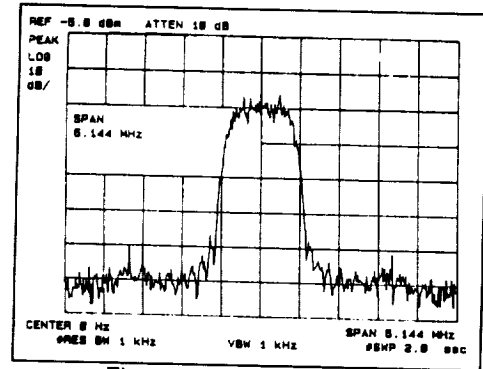


Figure 17: 8PSK Spectrum

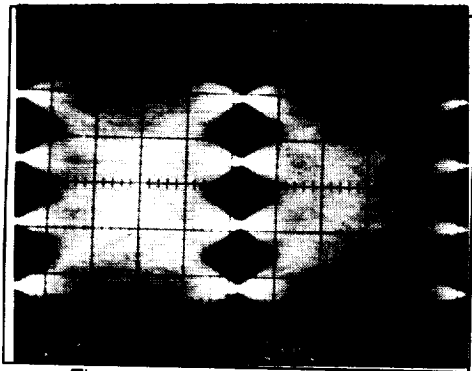


Figure18: 16 QAM Eye Diagram

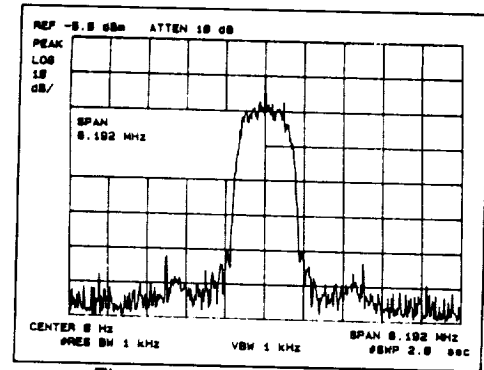


Figure 19: 16 QAM Spectrum

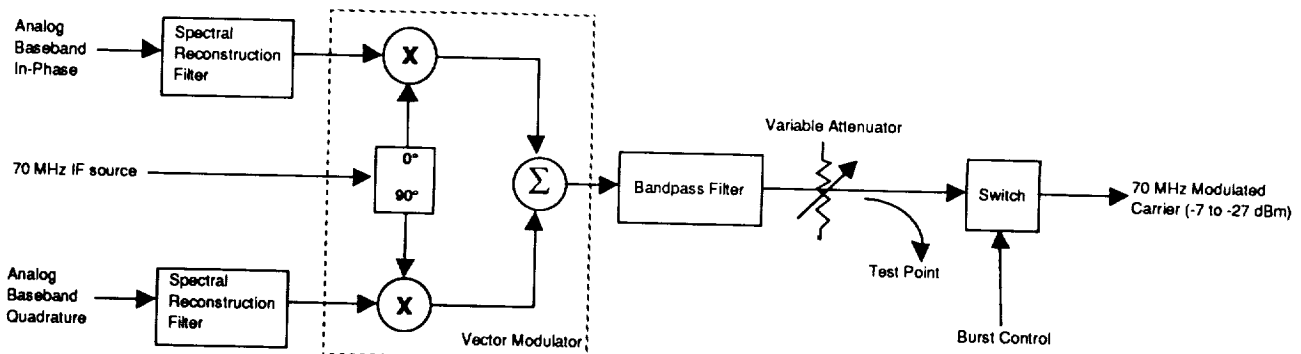


Figure 20 : Analog IF Upconversion

15 nanoseconds up to 3.5 MHz. This means that 40 percent Nyquist filters (cutoff approximately 3.5 MHz) will have a group delay over their entire bandwidth of no more than

$$\tau_{\max} = \frac{\tau_{\max \text{ symbol BW}}}{T_{\text{symbol max}}} = \frac{15 \text{ nS}}{200 \text{ nS}} = 7.5 \%$$

for the worst case symbol rate of 5 Msps. This effect causes an expected E_b/N_0 degradation of no more than a few tenths of a dB.

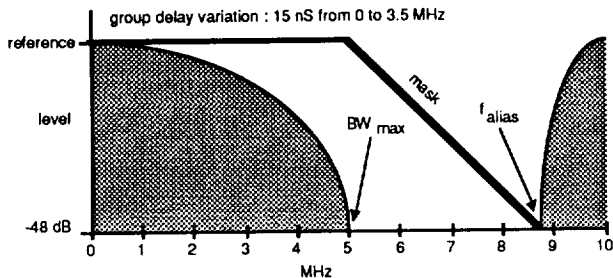


Figure 21 : Spectral Reconstruction Filter Mask

CONCLUSION

The architecture and hardware prototype of a flexible trellis-coded modem and codec transmitter has been presented. The FTMC transmitter uses digital modulation and coding, multi-symbol digital pulse shaping, and digital precompensation to tradeoff complexity for improved signal quality, bandwidth, and power efficiency. This type of architecture is envisioned to be of use in FDMA satellite uplinks and TDM or CDM satellite downlinks.

In any planned operational satellite network, the choice of modulation and coding techniques is dictated heavily by numerous other system concerns. However, offering future system designers workable flexible modems and codecs may relieve specifications in other subsystems and offer an enhanced satellite system that can offer more varied and higher quality services.

ACKNOWLEDGEMENT

The authors would like to thank L. Shimoda of Ohio University for generating the simulation data for Figures 8 through 11.

REFERENCES

[1] Viterbi, A. J., et al: A Pragmatic Approach to Trellis-Coded Modulation. IEEE Communications Magazine, July 1989, pp. 11-19.

[2] Harrold, J. L.; Budinger, J. M.; and Stevens, G. H.: On-Board Switching and Processing, Proc. IEEE, vol. 78, No. 7, July 1990, pp.1206-1212.

[3] Nuspl, P. P., et al: On-board Processing for Communications Satellites : Systems and Benefits, International Journal of Satellite Communications, Vol. 5, 1987, pp. 65-76.

[4] Campanella, S. J.: Communications Satellites: Orbiting into the 90's, IEEE Spectrum Magazine, August 1990, pp. 49-52.

[5] Hansen, J. W., et al: US TWTs from 1 to 100 GHz, Microwave Journal • 1989 State of the Art Reference, pp. 179- 193.

[6] Saha, D.; and Birdsall, T. G.: Quadrature-Quadrature Phase-Shift Keying, IEEE Transactions on Communications, Vol. 37, No. 5, May 1990, pp. 437- 448.

[7] Sklar, B.: Digital Communications Fundamentals and Applications, Prentice Hall, 1988.

[8] Lee, P. J.: Computation of the Bit Error Rate of Coherent M-ary PSK with Gray Code Bit Mapping, IEEE Transactions on Communication, Vol. 34, No. 5, May 1986, pp 488- 491.

[9] Poklemba, J. J: Programmable Digital Modem, NASA Space Communications Technology Conference, November 1991.

[10] Aghvami, A. H.; and Gemikonakli, O.: 16-ary QAM System for Low Data-Rate Satellite Services, Electron. Lett., Vol. 25, No. 16, August 3, 1989, pp. 1055- 1056.

[11] Allan, R. D.; Bramwell, J. R.; and Tomlinson, M.: A High Performance Satellite Data Modem Using Real-Time Digital Signal Processing. Olympus Utilisation Conference, Vienna, Italy, May 1989, pp. 51-55.

[12] Karam, G.; and Sari, H.: Analysis of Predistortion, Equalization, and ISI Cancellation Techniques in Digital Radio Systems with Nonlinear Transmit Amplifiers.

[13] Biglieri, E.; Barberis, S.; and Catena, M.: Analysis and Compensation of Nonlinearities in Digital Transmission Systems, IEEE Journal on Selected Areas in Communications, Vol. 6, No. 1, January 1988, pp. 42- 51.

[14] Cheung, S. W.; Aghvami, A.H.: Performance of a 16-ary DEQAM Modem Employing a baseband or RF Predistorter Over a Regenerative Satellite Link, IEE Proceedings, Vol. 135, No. 6, December 1988, pp. 547- 557.

[15] Karam, G.; and Sari, H.: A Data Predistortion Technique with Memory for QAM Radio Systems, IEEE Transactions on Communications, Vol. 39 , No. 2, February 1991, pp. 336- 344.

REPORT DOCUMENTATION PAGE

Form Approved
OMB No. 0704-0188

Public reporting burden for this collection of information is estimated to average 1 hour per response, including the time for reviewing instructions, searching existing data sources, gathering and maintaining the data needed, and completing and reviewing the collection of information. Send comments regarding this burden estimate or any other aspect of this collection of information, including suggestions for reducing this burden, to Washington Headquarters Services, Directorate for Information Operations and Reports, 1215 Jefferson Davis Highway, Suite 1204, Arlington, VA 22202-4302, and to the Office of Management and Budget, Paperwork Reduction Project (0704-0188), Washington, DC 20503.

1. AGENCY USE ONLY (Leave blank)	2. REPORT DATE November 1991	3. REPORT TYPE AND DATES COVERED Conference Publication	
4. TITLE AND SUBTITLE Space Communications Technology Conference Onboard Processing and Switching		5. FUNDING NUMBERS WU-650-60-21	
6. AUTHOR(S)		7. PERFORMING ORGANIZATION NAME(S) AND ADDRESS(ES) National Aeronautics and Space Administration Lewis Research Center Cleveland, Ohio 44135-3191	
8. PERFORMING ORGANIZATION REPORT NUMBER E-6548		9. SPONSORING/MONITORING AGENCY NAMES(S) AND ADDRESS(ES) National Aeronautics and Space Administration Washington, D.C. 20546-0001	
10. SPONSORING/MONITORING AGENCY REPORT NUMBER NASA CP-3132		11. SUPPLEMENTARY NOTES Responsible person, James M. Budinger, (216) 433-3496.	
12a. DISTRIBUTION/AVAILABILITY STATEMENT Unclassified - Unlimited Subject Categories 17 and 32		12b. DISTRIBUTION CODE	
13. ABSTRACT (Maximum 200 words) This proceedings of the NASA Space Communications Technology Conference held on November 12-14, 1991, in Cleveland, Ohio, presents onboard processing and switching technologies for application in future satellite communications systems. Onboard processing for B-ISDN (broadband integrated services digital network) services, packet-switched FDMA/TDM (frequency division multiple access/time division), a novel variation of CDMA (code division multiple access), and the merits of OBP (onboard processing) for low Earth orbiting mobile systems are addressed in the section, Satellite Network Architectures. Telecommunications services for the next generation of networks, a traffic analysis of B-ISDN, advanced lightwave networks, and survivable system processing are covered in Network Control and Protocols. Papers on bandwidth efficient coding, artificial intelligence for Earth terminals, multicarrier demodulation, neural-network-based video compression, an expert system for fault diagnosis, and laboratory measurements of INTELSAT OBP subsystems are presented in Concurrent Poster Presentations and Demonstrations. Two papers on expert systems for space hardware diagnostics and fault tolerance applied to fiber-optic networks and multichannel demultiplexers are covered in Fault Tolerance and Autonomy. Digital, optical, and acousto-optical approaches to multichannel demultiplexing and demodulation for onboard processed FDMA are presented in Multichannel Demultiplexing and Demodulation. In Information Switching and Routing, an onboard baseband switch, an OBP payload for asynchronous relay satellite networks, OBP for future telecommunications services, and congestion control for satellite packet switching are presented. In Modulation and Coding, the final section of this document, advanced modulation and coding technologies are applied to a B-ISDN modem-codec, a flexible, high-speed codec, and two variable-rate digital modems. Decoding multilevel demodulation and two approaches to digital pulse-shaped modulation for nonlinear satellite communications are also presented. Papers for the final two sessions of the conference were not available at the time of publication. These sessions, which addressed planned communications satellite systems under development at INTELSAT, NASA, Motorola, and Space Systems/Loral, and a panel session on the issues and challenges of onboard processing and switching technology insertion, are covered in a companion publication.			
14. SUBJECT TERMS Onboard processing; Modulation; Coding; Autonomy; Switching; Routing; Network control		15. NUMBER OF PAGES 312	
16. PRICE CODE A14		17. SECURITY CLASSIFICATION OF REPORT Unclassified	
18. SECURITY CLASSIFICATION OF THIS PAGE Unclassified		19. SECURITY CLASSIFICATION OF ABSTRACT Unclassified	
20. LIMITATION OF ABSTRACT			

NSN 7540-01-280-5500

Standard Form 298 (Rev. 2-89)
Prescribed by ANSI Std. Z39-18
298-102

NASA-Langley, 1991

